Chapter 6

Modeling Friction for Turbomachinery Applications: Tuning Techniques and Adequacy Assessment of Heuristic Contact Models

Chiara Gastaldi

Additional information is available at the end of the chapter

http://dx.doi.org/10.5772/intechopen.72676

Abstract

Friction dampers are commonly included into turbine designs to limit the turbine blades resonant vibrations and thus avoid high cycle fatigue failures. In order to effectively predict the effect of friction dampers on the turbine dynamics, friction is included into the simulation through specific mesoscale contact models. These models require knowledge of contact parameters to offer meaningful predictions. Standard single-contact test arrangements may fail to capture the true contact conditions and kinematics of friction dampers, especially for complex multi-interface contacts interested by variable normal loads. Several methodologies have been proposed in the literature: the lack of a "shared" approach in the field pinpoints a true "gap" in the research. Overcoming this difficulty is of primary importance, as it is the one feature that separates a state-of-the-art numerical code from a true design tool. Purpose of this chapter is to illustrate the experimental/numerical tools and methods developed to fill this gap for a common family of friction dampers, called "underplatform dampers" with a curved-flat cross section. Both cylinder-on-flat and flat-on-flat interfaces are addressed. The adequacy of the state-of-the-art contact model is discussed on the basis of a large data set obtained performing an extended experimental campaign on multiple damper samples.

Keywords: contact modelling, contact parameters estimation, case studies, underplatform damper, friction damping

1. Introduction

High cycle fatigue failure is a primary concern among operators and suppliers of turbo engines because of their suddenness [1].

They are caused by the large response levels at resonance. Since turbine blades do not benefit significantly from material hysteresis and aerodynamic damping, the only option is to add external sources of damping, for example, in the form of dry friction devices [2, 3] such as the underplatform damper. Underplatform dampers, available in several shapes (cylindrical, curved-flat and wedge-like), are small metallic objects placed on the underside of two adjacent blades. As shown in **Figure 1a**, the centrifugal force (CF) provides the necessary precompression and the resonant-induced blade vibration triggers the damper-platform relative motion and therefore friction dissipation. Dampers are extensively used in turbine designs because they are easy to manufacture, install and substitute, while relatively inexpensive.

Whenever a damper is added to the bladed system, its dynamic response is modified into two fundamental ways:

- the blades' resonant frequencies increase since the damper acts as an additional constraint (with a given stiffness) between the platforms and
- the blades' response diminishes for the combined effect of the stiffness introduced by the damper (which acts as a constraint) and of friction damping.

An additional complication is posed by the nonlinearity introduced by friction: it is well known that the non-linear dynamic response of bladed systems (both in frequency and maximum amplitude) is tightly coupled to the motion of the damper and its contact states (stick-slip-separation).

Accounting for the presence of friction is not an easy task. The presence of friction-induced nonlinearities makes solving the equilibrium equations a challenging task, therefore standard FE codes are not suited to the purpose: a complex hierarchy of techniques has been developed, a thorough review can be found in [4]. Furthermore, modeling friction entails:

1. finding a reliable model for the force-displacement relation at the contact interface and
2. a proper way to estimate its parameters.

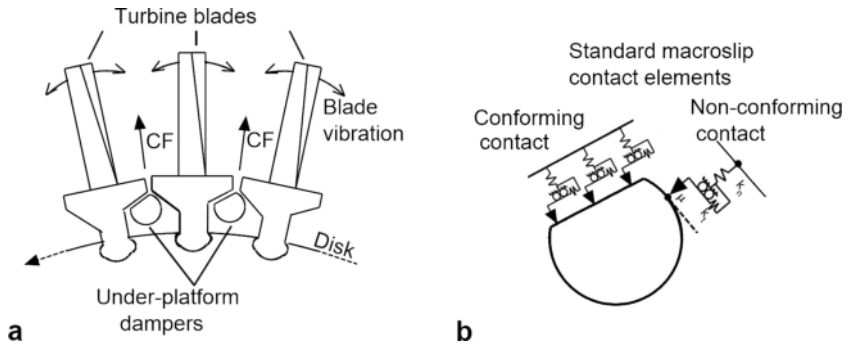

Figure 1. (a) Sketch representing curved-flat underplatform dampers mounted on a turbine disk. (b) Example of standard macroslip contact element used to represent conforming and nonconforming contacts.

1.1. A quick critical review of contact modeling in the turbomachinery field

In the technical literature, the problem of modeling periodical contact forces at friction contacts is still ongoing [5] and has been addressed by several authors, leading to different contact models and techniques. Some authors adopt a Dynamic Lagrangian method to solve on the contact patch [6, 7], that is, the contact constraints are taken into account in their non-regularized form without additional compliance. Other authors, for example, [4, 8] apply a contact element to each meshed node belonging to the contact area, introducing normal and tangential stiffnesses and a Coulomb friction law. This last method is preferred here, as its calibration parameters (k_n, k_t and μ), however difficult to determine, represent a physical measurable property.[1]

The contact elements typically used in turbomachinery belong to the "spring-slider" family, a class of displacement-dependent contact models which neglect features like viscous forces along the normal direction and friction's velocity-dependence. These features, while relevant in other fields, are not typically considered in turbomachinery applications. These models belong to the larger family of heuristic models, as opposed to microscale "realistic" models where asperities and surface roughness are modeled using stochastic distributions [9].

These interactions can be geometrically divided in the normal and the tangential directions. A unilateral contact law is often considered in the normal direction (with or without normal contact stiffness) and frictional law for the tangential contact. The spring-slider elements have undergone an evolution, starting from 1D tangential motion without normal compliance [2] up to a fully coupled 3D motion [10], passing through a 1D element with normal compliance (2D motion) [11]. This last element has been adopted by many authors because of its simplicity and versatility. In fact, it can be applied to represent 1D in-plane relative motion (a quite common occurrence if the first bending modes of the blades are considered), or, with a simple upgrade [12], to give a simplified representation of 2D in-plane motion.[2]

Modeling conforming (i.e. flat-on-flat) or nonconforming (e.g. cylinder-on-flat) surfaces requires a different strategy. Nevertheless, the same standard macroslip contact element presented in [11] can be applied (as it is done in this Chapter, see also **Figure 1b**).

Conforming contact surfaces are typically discretized into contact points (or nodes in FE terms) and each one is assigned a standard macroslip element, either with uncoupled 2D in-plane motion [8, 13, 14] or with a coupled one [15]. This choice allows to account for the presence of "microslip", first theorized by Cattaneo in 1938 [16], and later explored by Mindlin [17]. Modeling microslip is particularly relevant in those cases where high normal loads prevent actual slipping of the complete interface: in that case the gradual loss of stiffness that forecomes gross slip and the consequent dissipation does have an impact on the system response, while it becomes negligible if the gross slip regime is reached [18].

Nonconforming contacts are, in most cases, represented using one of the standard macroslip contact elements described above. Recently, a novel contact element, fit to take into account microslip as well as the nonlinearity in the normal direction typical of nonconforming contacts, has been proposed [18].

---

[1]Furthermore, Herzog et al. [7] have shown that Dynamic Lagrangians may incur in convergence problems for penalty parameters lower than 107 N/m, thus highlighting a possible limitation of their use in case of "softer" contact interfaces.
[2]Where the 2D tangential motion is albeit considered as the combination of two uncoupled 1D motions.

Other ad-hoc elements built to take into account microslip exist [19–24], however they are typically applied to conforming surfaces, which is somewhat limiting, as the kinematics of the contact, which play a significant role in the non-linear dynamic behavior, are not well represented.

1.2. A quick critical review of contact parameter estimation

All contact models require knowledge or information of contact-friction parameters to provide meaningful predictions.

Realistic models, based on the integration over the whole contact surface of mechanical principles applied at the asperity level, for example [9], are the only kind which allow for a predictive contact parameter estimation. In other words, these models can be calibrated using information concerning the geometry, roughness distribution, material properties, etc. Unfortunately, at least in many applications such as the turbomachinery field, this level of refinement has not yet been achieved and heuristic models are preferred.

Heuristic models are instead based on phenomenological friction laws (e.g. Coulomb's friction law), and their calibration is based on fitting to empirical observations.

Taking a state-of-the-art macroslip contact model with normal compliance described in Section 1.1, the parameters to be determined are normal and tangential contact stiffness k_n and k_t and friction coefficient μ.

The first, and perhaps, most obvious choice, is the use of single-contact test arrangements capable of providing the hysteresis cycle at a given (constant) normal load. Friction coefficients can be easily determined taking the ratio of the limit value of the tangential friction force during slip and the corresponding normal load [5, 25]. Tangential contact stiffness k_t [2, 25–27] can be estimated by taking the slope of the hysteresis curve in stick condition. This methodology is effective, as it can explore different temperatures, mean normal loads and frequencies. However, as will be shown in the following sections, it may fail to capture the true contact conditions and kinematics, especially for complex multi-interface contacts such as underplatform dampers.

Other methods are available, especially for the determination of contact stiffness values.

1. A complete analytical solution (k_n and k_t) is available only for circular or elliptical contact areas (i.e. Hertz theory), thus of limited interest in turbomachinery applications, while the normal compliance (k_n) is available for cylinder-on-flat contacts [28].
2. Another possibility is to mimic the single-contact tests using non-linear FE analysis [29]: two contacting bodies are modeled using a very fine FE mesh and each node is assigned a Coulomb-like slip criterion. Stiffness values are evaluated from computed force-deformation curves. Results were found to be 6–11% higher with respect to measured counterparts, possibly because of *"the neglected surface roughness as well as adhesive contact and viscous-elastic solid behavior"* [30].
3. In 2002, the "residual stiffness" method was proposed [31]. It is based on the observation that typical reduction techniques (e.g. CB-CMS [4]), used to reduce the size of FE models, may neglect the small local deformations. A "correction factor" is introduced to take into

account this effect. Unfortunately, a study performed in [32] suggests that this method gives a poor estimation of the contact stiffnesses.

4. In 2009, Allara [33] proposed a model to determine k_n and k_t of a 3D flat indenter with rounded edges pressed against an infinite half-plane. However, its results were found to be overestimating observed compliances [34].

5. The last (and perhaps the most popular) method is based on tuning against experimental [35] or numerically obtained [36] Frequency Response Functions (FRFs). Contact stiffness values are tuned until the experimental (or full FE model) evidence and that obtained from the reduced model with contact elements match. This operation is performed using evidence in full stick condition, so that all contact stiffness are "active" and accounted for.

One common point to approaches 2, 3 and 5 is that they use, as a benchmark, the solution offered by the full model in the FE software environment. This implies relying predictions performed with the Penalty or the Augmented Lagrangian Method to enforce the impenetrability condition and neglecting the possible influence of surface roughness.

Using, as a benchmark, numerical evidence is certainly quite convenient, as it does not require experiments and it is generally quite "complete" (the user can interrogate the software and retrieve displacements, stresses at any point of the mesh). However, it is based on the strong assumption that sees the full FE model as representative of the true contact conditions.

Approach 5 is usually regarded as the fastest and most effective, as it guarantees that the simulated target evidence matches the reference one. However, this local adjustment of parameters does not truly add knowledge to the field. In fact, it has a strong ad-hoc character, and must be repeated for every new system the designer comes across.

Another possible "drawback" of approach 5 is the possible under-determinacy of the contact parameter problem. As shown in [37], there exist multiple combinations of contact parameters capable of satisfying a given FRF. Therefore, if the number of contact parameters to be determined is larger than the (observed or computed) target features to be matched during tuning (or the influence of contact parameters is weak on the available target features), multiple solutions are possible. Two sets of contact parameters which produce equivalent responses at a given excitation level, may give rise to radically different solutions if the excitation level changes (see **Figure 1**, for example, with a curved-flat damper between a set of blades). This may not be a critical issue if a large number of target evidence can be produced (e.g. if the reference evidence is obtained numerically) and/or if the contact parameters to be determined are limited. However, it becomes a strong limitation if curved-flat underplatform dampers, characterized by a complex kinematics and multiple contact interfaces, are considered.

For all these reasons, it is here believed that the contact parameter estimation problem should be tackled using dedicated experimental evidence which focuses on the damper-blade interface. An increased attention to the damper kinematics has been demonstrated by other notable researchers in the field: in detail in [8] laser measurements have been employed to record damper rotation, while in [38] Digital Image Correlation has been used to investigate contact displacements.

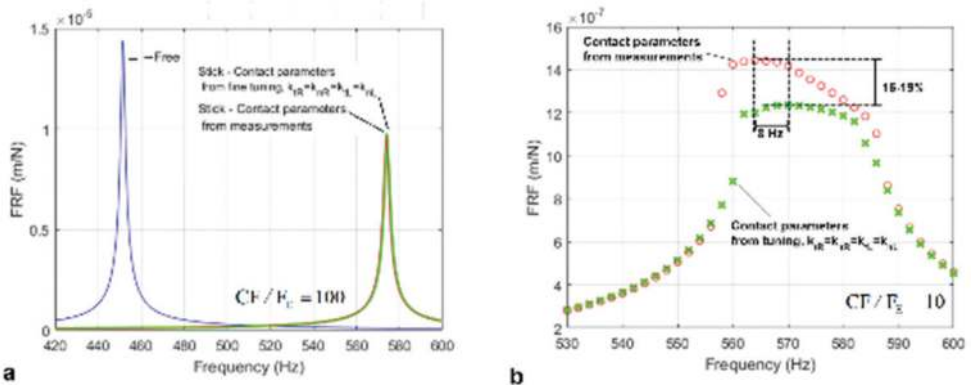

Figure 2. (a) Example of tuning of contact parameters in the full stick regime: two sets of contact parameters (one from Section 3 and one with a simplified assumption) leading to the "same" FRF. (b) Resulting FRFs (excitation level out of the tuning range) produced by the two sets of contact parameters from **Figure 1a**. CF: centrifugal force on the damper, F_E: external excitation on blades.

1.3. Goals of the chapter

The main purpose of this chapter is to present the latest advances made by the AERMEC lab to improve the fidelity of damper modeling and to rigorously assess processes needed for reliable predictions/estimation of contact parameters (see **Figure 2**).

In detail, Section 2 briefly describes the Piezo Damper Rig (see **Figure 3a**), first presented in [39], and recounts its latest improvements.

Section 3 with reference to Section 1.1, defines a numerical damper model (also represented in **Figure 3b**) and justifies all modeling choices.

Section 3.2 uses the experimental evidence gathered on the above-mentioned rig to estimate all contact parameters necessary to represent a curved-flat damper between a set of platforms (conforming and nonconforming surfaces both).

In Section 4, the adequacy of the chosen contact model is discussed on the basis of an experimental campaign on numerous damper samples. Furthermore, the role of rotation of nonconforming contacts, a topic which has never been addressed in this context to the author's knowledge, will be explored.

The chapter conclusion (Section 5) includes a series of warning and recommendation for the damper designer/tester.

2. Experimental evidence

The majority of the rigs developed to test underplatform dampers see a bladed system (equipped with dampers) excited at resonance [8, 35]. Often, the FRF of the system is used as

the sole indicator of the damper performance. The FRF is certainly an important design indicator, however by itself, it is not capable of offering enough information on the damper working conditions. Furthermore, if FRFs are the only experimental evidence available it is likely that, as pointed out in Section 1.2, the contact parameter problem will remain underdetermined.

2.1. The Piezo Damper Rig

For all these reasons, in 2009, the AERMEC lab proposed a novel kind of test rig (see **Figure 3a**) which focuses directly on the underplatform damper. No blades are present (i.e. it is not a resonant rig). On the other hand, two dummy platforms are used to connect the system to the input motion generation and to the force measuring mechanism.

- The left platform is connected to two piezoelectric actuators inserted into a purposely designed mechanical structure. This system allows imposing any user-defined in-plane displacements simulating the so-called In-Phase (IP, vertical) and Out-of-Phase (OOP, horizontal) relative motion between the blades platforms or combinations of the two.
- The right platform is connected to two uniaxial force sensors by means of a tripod structure to the purpose of measuring the forces transmitted between the two platforms through the damper.

The damper is pulled by a deadweight simulating the centrifugal force, CF. The main purpose of the rig is to relate contact forces to the displacements that produce them (see also **Figure 3c**). For this reason, a differential laser head is employed to measure the platforms relative displacement (a necessary precaution owing to the lack of closed loop control of the piezoelectric actuators), the damper radial displacement and rotation angle and the damper-platform relative displacement at the contact. A scheme representing the laser positioning to obtain the tangential relative motion at the contacts and the damper rotation is shown in **Figure 3d**.

2.2. The test rig evolution

The key features of the test rig described above remain unchanged since its first version [39], however several subsequent improvements have been performed (see **Figure 4** for a graphical representation). In detail, the tripod and the structure hosting the force sensors have been redesigned to increase the overall stiffness of the rig [18]. This had a positive impact over the frequency operating range which increased from [≈5–80] Hz to [≈5–160 Hz]. In [40] each platform has been redesigned into two parts: a "fixed" part connected to the rest of the test rig (the left platform to the actuators, the right one to the force sensors) and a second part, termed here "insert" in contact with the damper. This configuration has several advantages: (i) the "insert" can be substituted to test different platform angles, (ii) the contact is localized along the damper axis by means of 4 mm wide protrusions present on both platform inserts which ensure high contact pressures even with moderate deadweights on the damper.

Lastly, the new platform inserts and dampers have been machined with cube-like protrusions oriented with one of the faces perpendicular to the contact line. Each contact line (left and right) is equipped with two cubes (one on the damper and one on the corresponding platform).

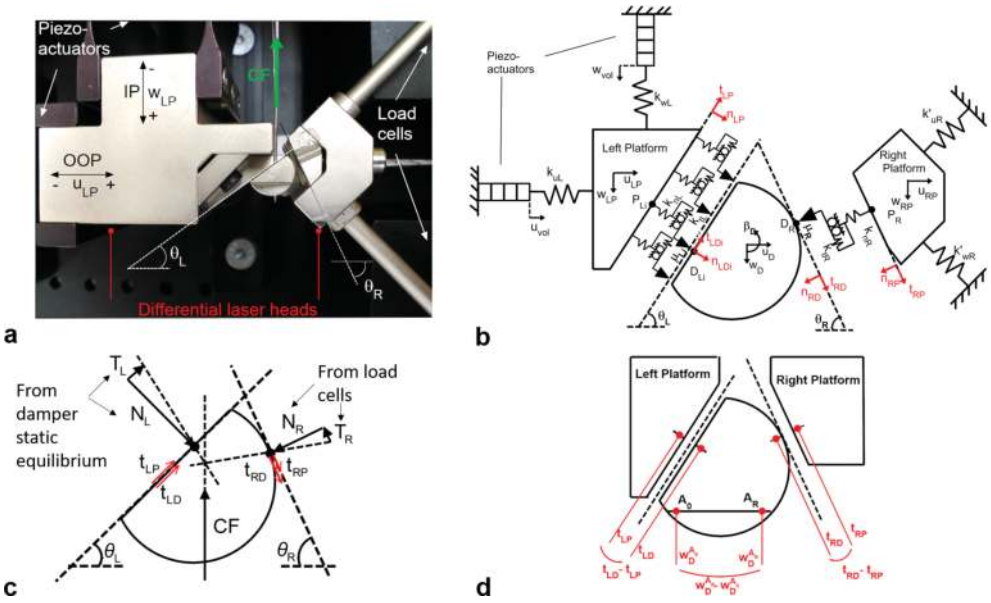

Figure 3. (a) Piezo Damper Rig scheme and relevant quantities. (b) Piezo Damper Rig numerical model. (c) Measured and derived contact forces. (d) Laser positioning to obtain relevant kinematical quantities.

Diagram	Goal	Quantities	Measurement technique	Uncertainty
T/N force ratios (**Figure 5a**)	Estimate friction coefficient	T_R/N_R	Derived	3–5%
	Identify contact states	T_L/N_L	Derived	6–10%
Hysteresis at nonconforming contact	Estimate tangential contact stiffness	t_{RD}-t_{RP}	Laser vibrometer	0.08 μm (~0.2%)
		T_R	Load cells	2%
Hysteresis at conforming contact (**Figure 5b**)	Estimate tangential contact stiffness	t_{LD}-t_{LP}	Laser vibrometer	0.08 μm (~0.2%)
		T_L	Derived	2.5%
Moment vs. Rotation diagram (**Figure 5c**)	Estimate normal contact stiffness (conf. contact)	β_D	Derived[1]	5%
		$M = N_L * x$	Derived	5–7%
Platform-to-platform hysteresis cycle (**Figure 5d**)[2]	Validation	w_{LP}-w_{RP}	Laser vibrometer	0.08 μm (~0.2%)
		V_R	Load cells	2%
Contact forces diagram (**Figure 6a**)	Validation, check position of left contact force	T_R, N_R		2%
		T_L, N_L, application point		2.5%, <1 mm

[1]Damper rotation is here obtained as described in, that is, with reference to **Figure 3d**, $\beta_D = \left(w_D^{A_0} - w_D^{A_R}\right)/\overline{A_0 A_R}$.

[2]This example is carried out in case of IP motion, a similar diagram can be obtained in case of OOP motion by plotting the horizontal force component H_R against the corresponding horizontal platform relative displacement $u_{LP} - u_{RP}$.

Table 1. Essentials in damper diagrams.

This allows for the direct measurement of the tangential relative motion at the contact (as shown in **Figure 3d**): this constitutes a true improvement in the test rig capabilities since it allows, as described in Section 3, for the estimation of the tangential contact stiffness values.

2.3. Measurement protocol

Each experimental nominal condition is defined by: damper configuration (i.e. shape, platform angles, etc.), centrifugal load on the damper, excitation frequency, amplitude and direction of motion.

The analysis of the damper performance under each nominal experimental condition is operated through the cross-comparison of a series of quantities (whose graphical representation can be found in **Figure 3b–d**) organized into diagrams (summarized in **Table 1**, shown in **Figures 5** and **6** and further commented in Section 3.2). Both contact forces and damper/platform kinematics are taken into account for the purpose of uncovering the cross-relations existing between them and to estimate contact parameters. It should be noted that some of these quantities are directly measured (e.g. tangential and normal forces at the nonconforming contact T_R and N_R and all damper displacements), while other quantities are derived (e.g. tangential and normal forces at the conforming contact T_L and N_L are obtained through the damper equilibrium by neglecting inertia forces at frequencies where this is correct, as shown

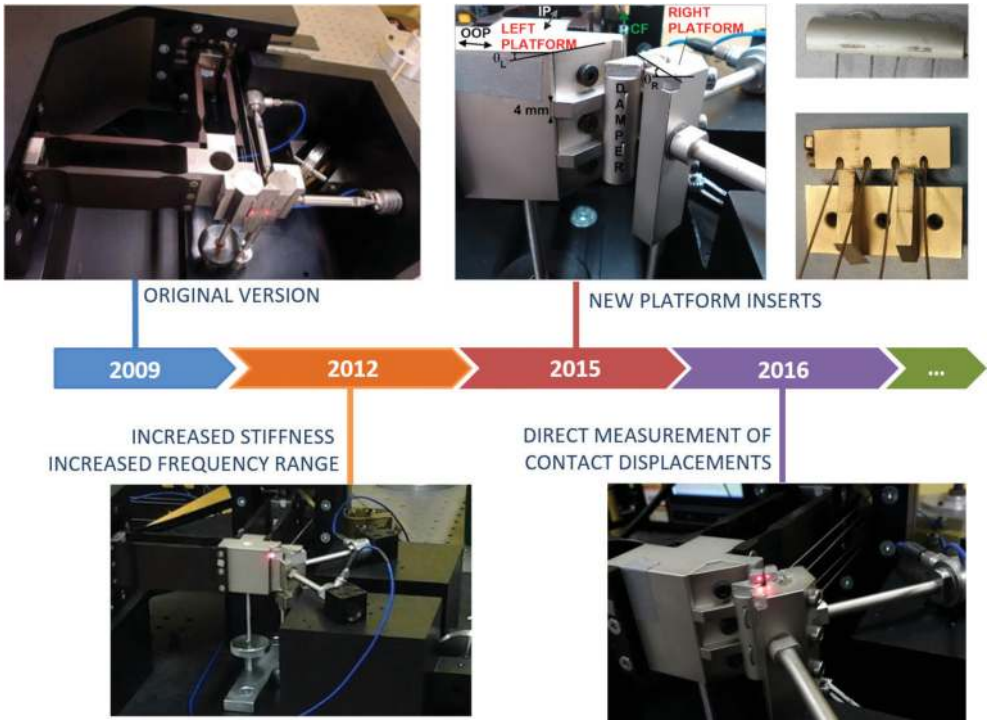

Figure 4. Piezo Damper Rig evolution.

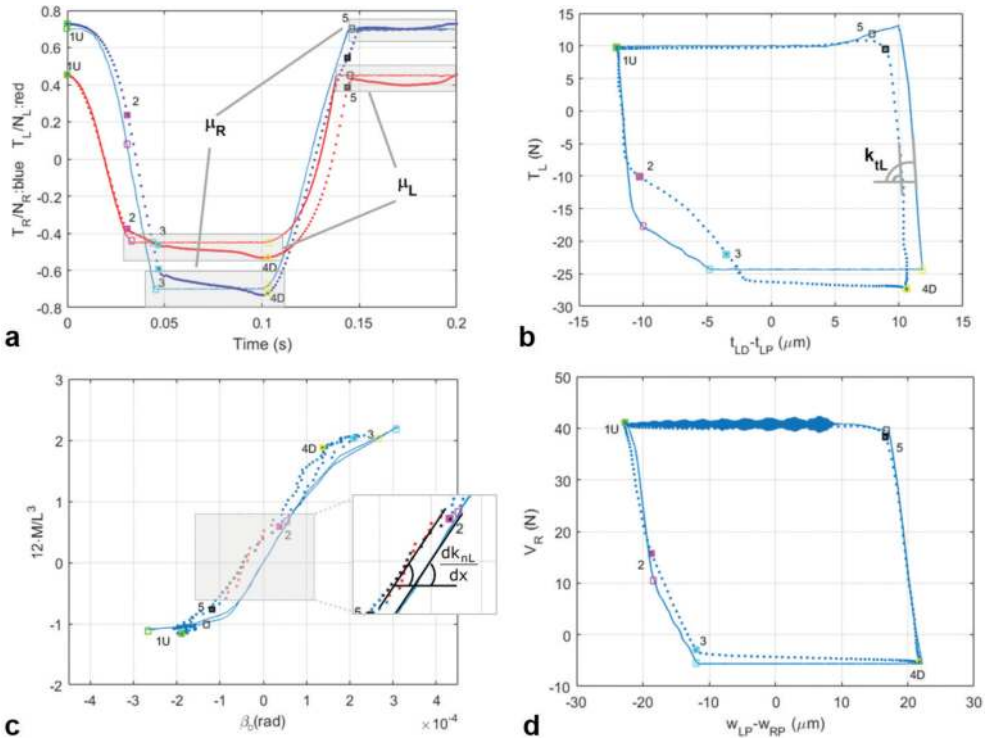

Figure 5. Measured vs. simulated. (a) T/N force ratio diagram. (b) Platform-to-damper hysteresis cycle at the flat-on-flat contact. (c) Moment vs. rotation diagram. (d) Platform-to-platform hysteresis cycle. Measured: dotted line, simulated: solid line. IP case, with CF = 4.65 kg.

in **Figure 3c**). Each quantity is equipped with a proper level of uncertainty. Measurement uncertainty, minimized through a purposely developed protocol, ensures significant trustworthy results (error up to 7%).

3. Numerical model and contact parameters estimation

The diagrams summarized in **Table 1** and shown in **Figures 5** and **6a** are represented together with the corresponding simulated counterpart, obtained using the numerical model shown in **Figure 3b**.[3] The numerical model represents the damper inside the test rig, however the same numerical routine can be incorporated into a code which substitutes the test rig presence with that of a FE bladed system [35].

[3]The springs representing the tripod and the mechanical structure hosting the piezo actuators have been experimentally measured as described in [39].

Only in-plane motion is addressed here (typical of blades bending modes, where dampers are most effective), however a more general 3D version of the same model is available for more complex cases. The general equilibrium equation to be solved at this stage is:

$$[M]\{\ddot{U}\} + [K]\{U\} = \{F_e\} + [T]\{F_C\} \tag{1}$$

where with reference to **Figure 3b**, $[M] = diag(m_D, m_D, m_D, m_{LP}, m_{LP}, m_{RP}, m_{RP})$, $[K] = diag(0, 0, 0, k_{uL}, k_{wL}, [k'_R])$ with $[k'_R] = \begin{bmatrix} k'_{uR}\cos^2\alpha + k'_{wR}\sin^2\alpha & (k'_{uR} - k'_{wR})\sin\alpha\cos\alpha \\ (k'_{uR} - k'_{wR})\sin\alpha\cos\alpha & k'_{uR}\sin^2\alpha + k'_{wR}\cos^2\alpha \end{bmatrix}$, $\{U\} = \{u_D, w_D, \beta_D, u_{LP}, w_{LP}, u_{RP}, w_{RP}\}$, $\{F_E\} = \{0, -CF, 0, k_{uL} \cdot u_{vol}, k_{wL} \cdot w_{vol}, 0, 0\}$, $\{F_C\} = \{T_R, N_R, T_{L1}, N_{L1}, \ldots, T_{Ln_c}, N_{Ln_c}\}$ and $[T]$ is a transformation matrix. In detail, vector $\{F_C\}$ is the output of the contact elements which are fed by the correct relative displacements at the contact.

In this chapter, Direct Time Integration [40] is used to avoid approximations, however should a larger system be considered, multi-Harmonic Balance Method can be applied [35].

The reader will notice that the damper is modeled as a rigid body, a quite reasonable assumption given the bulkiness of the damper.

The contact elements here applied are state-of-the-art in the gross slip regime [11], which is the focus of this chapter's investigation. The nonconforming contact (cylinder-on-flat) is modeled using one element, while the conforming contact requires at least two contact elements (four in **Figure 3b**). Increasing the number of contact elements will smoothen the hysteresis shape but not change significantly the damper behavior. The position of the contact points is typically set at equal intervals along the flat interface using the two edges as limits (i.e. starting and ending points).

3.1. Definition of the unknowns

In principle, friction is a material property, therefore all interfaces, both conforming and nonconforming, should share the same contact parameter values. Friction is indeed a material property at microscopical level, therefore if a reliable and validated "realistic" model was available one could start from material properties and surface characteristics, and integration over the contact area would do the rest. However, since the selected contact elements are of the "heuristic" kind, other factors influence k_n, k_t and μ values.

In detail previous experience has shown that the geometry of the contact surface (line vs. area contact), contact surface kinematics and normal load play a significant role [37]. The influence of normal load will be addressed in Section 4, while, in order to take into account the influence of the contact areas different geometries and kinematics, it holds:

$$\begin{aligned} k_{nR} &\neq k_{nL} \\ k_{tR} &\neq k_{tL} \\ \mu_R &\neq \mu_L \end{aligned} \tag{2}$$

for a total of six unknowns (also represented in **Figure 3b**).

Contact parameters of the flat-on-flat interface are typically distributed uniformly among the contact points, for example, considering the normal contact spring:

$$k_{nLi} = \frac{k_{nL}}{n_C} \tag{3}$$

The validity of this assumption will be further assessed in Section 4.

3.2. Step-by-step contact parameter estimation procedure

Contact parameters are estimated starting from the experimental evidence, organized into diagrams as summarized in **Table 1**. In detail, for a given experimental nominal condition:

Step 1. Reference points on the diagrams in **Figure 5** have been marked by a symbol and a number: they are useful to guide the analysis of the cycle through cross-comparison.

Step 2. The cross-comparison of the T/N diagram (**Figure 5a**) and of the observed relative displacement at the contact interfaces can be used to make a hypothesis on the contact states experienced by the damper during one period of vibration. Namely, if, during a given portion of the cycle, the T/N force ratio is constant and the relative displacement at the contact is non-negligible, then that interface is assumed to be in slip condition. On the other hand, if the T/N force ratio is varying and the corresponding displacement at the contact is negligible, the damper is likely to be stuck to the platform. This allows the user to assign each stage of a cycle a given contact state (see **Table 2**).

Step 3. Based on the results of **Table 2**, friction coefficients at the right (cylinder-on-flat) and left (flat-on-flat) interface, μ_R and μ_L, are estimated using the time history of the correspondent T/N force ratio during slip (see **Figure 5a**).

Step 4. Based on the results of **Table 2**, the slopes of the platform-to-damper hysteresis cycles (referring to the stages identified as being in stick condition) can be used to estimate tangential contact stiffness values (k_{tR} and k_{tL}).

Step 5. The normal contact stiffness at the cylinder-on-flat interface k_{nR} is estimated using Brandlein's formula [28]. To this purpose only material properties and length of contact are needed. The new inserts equipped with contact "tracks" described in Section 2.2 ensure a controlled length of contact.

	Right interface			Left interface		
Stage	**T/N slope**	**Δt_R[1] (μm)**	**Contact state**	**T/N slope**	**Δt_L (μm)**	**Contact state**
1U–2	High	~1	Stick	High	1.8	Stick
2–3	High	<0.2	Stick	Medium	7.8	Partial slip
3–4D	Low	21.3	Slip	Low	13.1	Slip
4D–5	High	−0.6	Stick	High	−1.7	Stick
5–1U	Low	−21.7	Slip	Low	−21.03	Slip

[1] Δt_R of stage, for example 2–3, is defined as $\left(t_{RD}(\tau_3) - t_{RP}(\tau_3)\right) - \left(t_{RD}(\tau_2) - t_{RP}(\tau_2)\right)$, where τ is the time variable.

Table 2. Experimental contact states identification strategy.

The distribution of the normal contact stiffness at the flat-on-flat interface per unit length dk_{nL}/dx is obtained by linking the damper inclination (i.e. rotation angle β_D at a given instant in time) to the position of the left contact force resultant N_L. In other words, it is postulated that forces (i.e. moments) and displacements (i.e. rotation) are linearly linked. The technique also relies on two assumptions: (1) the normal contact stiffness is uniformly distributed along the flat interface (see Eq. 3 and **Figure 6b**); (2) the force per unit length q(x) related to the normal component of the left contact force resultant N_L has a linear distribution. In detail, with reference to **Figure 6b**, let us define a reference system x, parallel to the contact with its origin in O, the mid-point of the flat interface. As shown in **Figure 6a**, the normal component of the left contact force resultant N_L travels along the flat surface during the cycle. If, however N_L enters the inner third portion of the flat interface (see **Figure 6c**) the complete surface is in contact. Under this condition, the following holds:

$$M = N_L \cdot x = \frac{d\,k_{nL}}{dx}\frac{L^3}{12}\beta_D \tag{4}$$

This relation is graphically represented in **Figure 5c**, where the shaded are corresponds to the portion of the cycle during which N_L enters the inner third portion of the flat interface.

3.3. Remark on experimental evidence and validation

All experimental evidence shown and commented in this chapter has been represented together with its simulated counterpart for validation purposes. Some of the features of the diagrams (i.e. T/N levels during slip stages and slopes of the hysteresis cycles during stick stages) are meant to be similar because they are used as a calibration key in the contact parameter estimation process. Other features such as force trajectories and left contact force resultant application point (**Figure 6a**); the platform-to-platform hysteresis cycle (e.g. **Figure 5d**); the transition between contact states and the time instant at which they take place (e.g. **Figure 5a**); are not part of the calibration process. Therefore, the goodness of fit of these observed and simulated signals is a further proof of the soundness of the model and of the correctness of the contact parameters used to calibrate it.

4. Contact parameters variability and contact model adequacy

The purpose of this section is to detail the level of uncertainty of each of the contact parameters estimated in Section 3.2 and to investigate their variability. Results are summarized in **Table 3** and will be further commented on in the following subsections.

Contact parameter	μ_R	k_{tR} (N/μm)	μ_L	k_{tL} (N/μm)	dk_{nL}/dx (N/m^2)
Uniform flat contact uncertainty bands	[0.6–0.75]	[25–35]	0.45–0.5	[20–30]	[0.8–1.2] × 10^{10}
Irregular flat contact uncertainty bands	[0.6–0.75]	[25–35]	0.45–0.6	[20–100]	[0.4–1.2] × 10^{10}
Normal load dependence	No	No	Yes	Yes	Yes

Table 3. Uncertainty bands and normal load dependence of contact parameters obtained at CF = 4.65 kg.

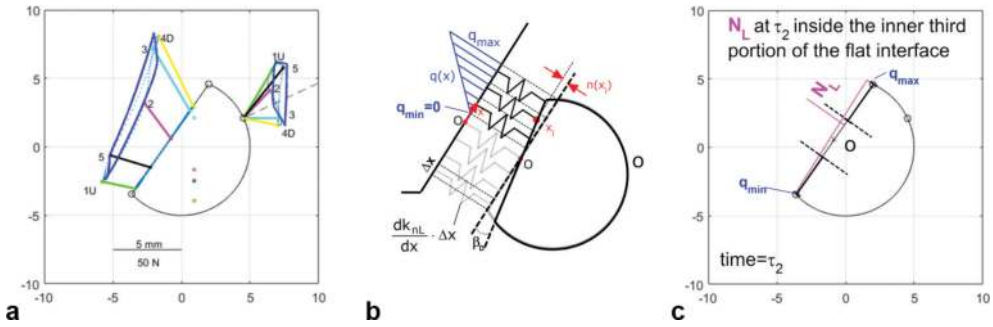

Figure 6. (a) Measured (dotted) vs. simulated (solid) contact forces diagram. (b) Representative scheme of the distribution of normal contact springs. (c) Derived position of N_L and resulting q(x) at stage 2.

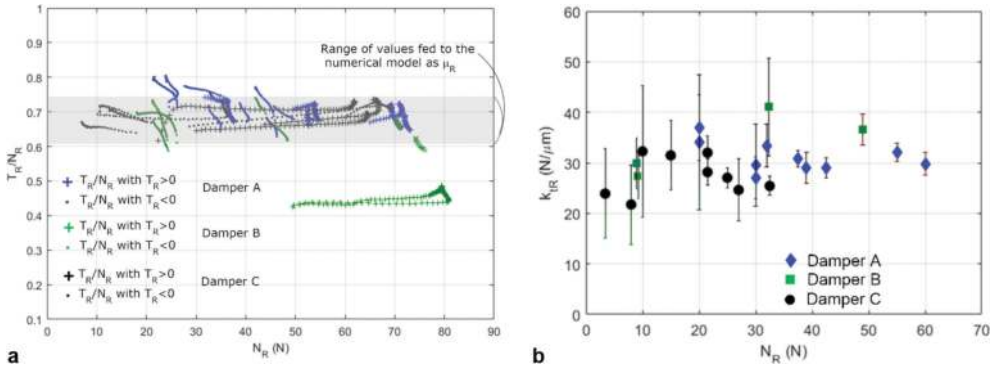

Figure 7. (a) T_R/N_R during slip as a function of N_R. (b) k_{tR} values as a function of the mean value of N_R during the corresponding stick stage. Three different damper samples are represented.

The level of uncertainty is estimated taking into account two contributions: measurement uncertainty and the uncertainty introduced by data processing techniques (e.g. reading error). Variability will be investigated at different levels in order to answer the following questions:

1. If the same damper is tested more than once under the same nominal conditions, do the estimated contact parameters change? 2. Are contact parameters dependent on the damper working conditions (e.g. normal contact pressure)?[4] 3. How different are contact parameters of different damper samples working under very similar working conditions?

The answer to point 3 is investigated using three pre-optimized damper configurations [40], that is, curved-flat dampers not affected by lift-off/rolling, jamming or partial detachment.

[4]The user-controlled working conditions investigated during this chapter are limited to a variation of centrifugal load on the damper (i.e. normal load at the contact). Other factors such as temperature, length/area of contact may affect the contacts. These dependences can and should be mapped in order to build a "database" and avoid testing each new component. This chapter should be intended as a first attempt in this direction.

4.1. Nonconforming (non-rolling) contacts

The uncertainty on μ_R is the combination of the uncertainty on T_R/N_R (3–5% from **Table 1**) and the reading error (typical values ≈ ±0.05 as shown in **Figure 5a**). The repeatability and sample-to-sample variability can be investigated by looking at **Figure 7a**.

Figure 7a shows the T_R/N_R force ratio during slip under increasing values of normal load N_R, achieved by increasing the centrifugal load (4.6–8.6 kg). Different dampers are represented with different colors and positive and negative slipping stages (see **Figure 7a** for sign convention) are represented using different symbols. "Clusters" of points of the same color and symbol belong to the same stage of the same experiment of the damper samples, represented with different colors.

Despite some inevitable variabilities (e.g. T/N ratios display minor variations during a single slip stage), μ_R can be set at a "unique value" for all investigated dampers. Furthermore, these variabilities are in the same range as the uncertainty introduced by the measuring and post-processing techniques. Choosing $\mu_R = 0.65$, a value mediated over all those encountered in **Figure 7a** is a perfectly adequate choice, which guarantees a controlled error on the equivalent stiffness and damping.

Similarly, k_{tR} (which is plotted as function of N_R in **Figure 7b**) is not influenced by the normal load[5] at the contact in the investigated range, is remarkably repeatable and no sample-to-sample variability is detected. In **Figure 7b**, the error bars are obtained by performing the least square fitting of the hysteresis slope.

It can therefore be concluded that contact parameters of the nonconforming contact are both repeatable and with a minor sample-to-sample variability.

4.2. Remark on rolling nonconforming contacts

The case of rolling contact is of scarce interest for curved-flat dampers, as it was demonstrated that large rotations (damper in lift-off) lead to a sharp decrease in dissipation capabilities [40]. However, purely cylindrical dampers are widely used and thus require a separate investigation.

The procedure to evaluate k_{tR} described in Section 3.2 cannot be operated if the damper is rotation is large (~10 times higher than that observed in **Figure 5c**). In fact, in that case, the reading "t_{RD}-t_{RP}" would give a false indication. As shown in **Figure 8a**, the laser, which is initially tracking point A ends up tracking point A*. However, the physical point initially corresponding to A is now A′, not A*. This apparently minor difference, at micrometer level, impairs the effectiveness of this technique.

Fortunately, an alternative procedure based on the equivalent slopes of the platform-to-platform hysteresis cycle can be successfully carried out, both for cylindrical dampers and for curved-flat dampers [37, 39]. It is interesting to notice that the resulting k_{tR} values are 3.5–4 times lower than those obtained for non-rolling cylinder-on-flat contacts, all other parameters

[5]This is to be expected, as the cylinder-on-flat surface has a line contact, and an increase in normal load will lead to a number of asperities coming into contact which is proportionately much smaller than that obtained for a rectangular contact area (flat-on-flat contact).

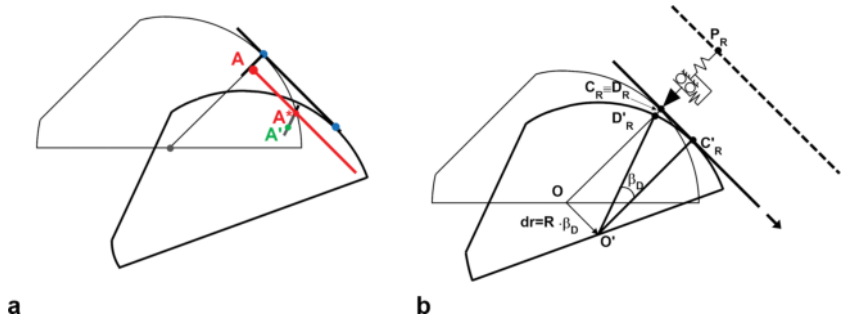

Figure 8. (a) Error committed by laser in case of large rolling motion mixed with sliding. (b) Behavior of the contact model in case of pure rolling motion.

(material, length of contact, radius, normal load, etc.) being equal (i.e. 8.5 N/μm vs. 30 N/μm for a 8 mm long contact). These predictions have been successfully validated both at damper [37] and at FRF level [34]. A possible explanation for this repeatable difference resides in the kinematics of the contact. In case of pure tangential translation (~0 rotation) the contact point coincides with the same physical point (same asperities) throughout the period of vibration. If larger rotations are at play, the "physical point" in contact keeps changing during rolling motion (as shown in **Figure 8b** contact point C_R initially coincident with physical point D_R, moves to C_R' and D_R, unloaded, moves to D_R'). This periodic unloading of contact regions may contribute to lower compenetration of the asperities, and therefore a lower k_{tR}. As shown in **Figure 8b**, the heuristic contact model applied here does not model this effect, therefore a case-specific calibration of k_{tR} is to be expected. In fact, during pure rolling motion, the contact model remains linked to the same nodes (physical points) P_R and D_R~D_R'.

4.3. Conforming contacts

Friction coefficient (μ_L) and contact stiffness values (k_{tL} and dk_{nL}/dx) of the flat-on-flat interface display a higher variability. Results for the same damper are very repeatable, but change from damper to damper.

Dampers B and C have repeatedly higher $\mu_L \approx 0.57$ with respect to Damper A, $\mu_L \approx 0.45$ (for all investigated normal loads) and the uncertainty levels (7% uncertainty and a 0.05 reading error) do not justify this marked and repeatable difference. Since the loading condition and kinematics of the flat interfaces are similar in all investigated cases, the cause of this difference may reside in the contact surfaces conditions.

In fact, Damper A, which has been tested for a higher number of cycles (it is completely "run-in") has a continuous wear trace (see **Figure 9c**). Unsurprisingly, it is easy to estimate k_{tL} (see **Figure 5b**). The same holds for dk_{nL}/dx (see **Figure 5c**) values. In other words, the uniform distribution of contact springs postulated in Section 3, is verified. Although both k_{tL} and k_{nL} values are positively correlated to normal loads (see **Figure 9a**). The adopted heuristic model does not take into account an increasing number of asperities coming into contact with increasing contact pressures. However, the normal load dependence can be easily mapped.

http://dx.doi.org/10.5772/intechopen.72676

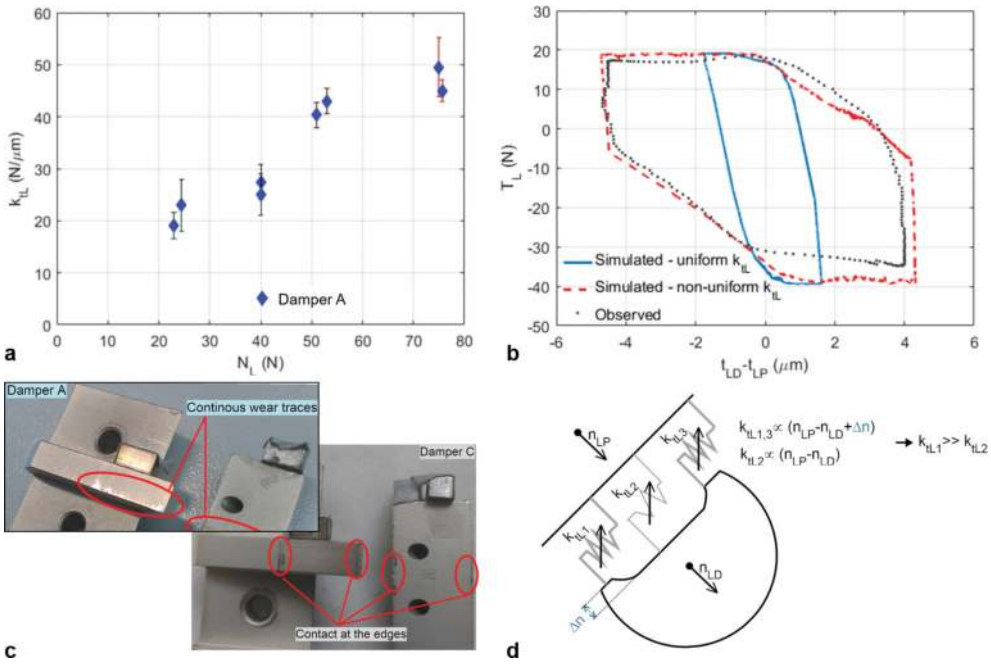

Figure 9. (a). k_{tL} as a function of N_L for Damper A. (b) Typical platform-to-damper flat-on-flat hysteresis cycle for damper C (similar to Damper B). (c) Contact surfaces of Damper A and C. (d) Representative scheme of Damper C's contact surfaces with non-uniform k_{tL} values.

On the other hand, Dampers B and C sport wear traces limited to the edges of the flat contact surfaces (see **Figure 9c**), therefore contact pressures are maximum at the two edges and much lower in the inner portion of the contact patch. As a result, friction coefficients increase (probably due to localized very high contact pressures) and the uniform distribution of contact springs assumption does not hold anymore. In fact, platform-to-damper hysteresis cycles (see **Figure 9b**), repeatedly display a non-unique slope during the stick stage. A minor gradual loss of stiffness could be explained by simple microslip, but this sharp two-slopes curve is simply not compatible with the uniform distribution of contact springs assumption.

Hysteresis cycles similar to those obtained for Dampers B and C can indeed be obtained in the simulation if one accepts to distribute the contact stiffness values in a non-uniform manner (see **Figure 9d**). The average height of Damper C's asperities is not the same throughout the entire nominal contact surface, rather it has two maxima at the edges. Therefore, for a given normal load, the equivalent stiffness at the edges is bound to be higher than that in the inner portion of the nominal contact surface. Therefore, if one wishes to represent the surface behavior with a limited number of equivalent macroslip elements the only option is to assign a different value to the different elements, depending on their position, as shown in **Figure 9d**. This strategy has been adopted to produce the very satisfactory match in **Figure 9b** (see dashed line). The procedure will have to be performed again if the mean value of normal load varies. Once again this "local fitting" (stiffness values vary with normal load and with

position now) denounces the inadequacy of the contact model. The inadequacy of the model forces the user to tune the contact stiffness values with increasing values of CF and, in some cases, with the contact point position.

5. Conclusions

A thorough review of contact models available for turbomachinery applications and the related calibration methods highlights the need for a method to solve the under-determinacy of the contact parameter estimation problem and, subsequently, to assess the adequacy of contact models. This chapter presents the evolution of the Piezo Damper Rig, a test facility for the experimental investigation of underplatform dampers. It was shown how its unique capability to provide kinematic and force related quantities while reproducing the real damper-platform kinematics allows for a trustworthy and univocal determination of contact parameters.

The measurement protocol and data processing technique ensure adequate uncertainty levels (i.e. <15%). The results can thus be used to perform safe and meaningful investigations on trends and variability of contact parameters.

The following conclusions can be drawn:

- independent experiments performed in the same nominal conditions (same damper, excitation, load etc.) are repeatable and consistent;
- contact parameter of nonconforming contacts display a remarkably low variability. No dependence on the contact pressure has been detected;
- contact parameters of conforming contacts display a higher variability caused by a difference in the surface conditions. In all cases, contact stiffness values increase with increasing contact pressures;
- the uniform distribution of contact stiffness along the flat contact surface, postulated in Section 3, is found to be adequate for run-in uniform surfaces (i.e. Damper A), but not for surfaces whose contact is “irregular” or “discontinuous”.

Heuristic models and sensible assumptions such as the uniformity of conforming contacts are nowadays considered a practical and adequate choice in turbomachinery applications. This is generally true, however special attention is required whenever a microscale phenomenon (e.g. nonuniform flat-on-flat contact, large rolling motion), not taken into account by the model, becomes prominent.

It was shown that the state-of-the-art heuristic contact model adopted in this chapter represents faultlessly run-in uniform flat-on-flat surfaces (i.e. Damper A). The same contact model CAN still be adapted to achieve simulated results matching the experimental evidence on dampers with irregular flat-on-flat contacts, but recalibrations are needed. For instance, a non-uniform distribution of k_{tL} among contact points, adjustments of the dk_{nL}/dx and μ_L values. Unfortunately, at design stage, when it is not possible to know “a-priori” the condition of

a given flat-on-flat contact surface, nor how long it will take for that surface to evolve towards a uniform distribution of contacts, this necessity for "adjustments" of contact parameters values translates into higher uncertainty levels. In other words, the state-of-the-art contact model used in this chapter is only partially adequate to represent all the complex phenomena observed. This adds its contribution to uncertainty.

On the other hand, other recalibrations (such as that needed for increasing normal loads at the flat-on-flat contact) or for very large rolling motions still signal that the heuristic model is not 100% adequate. Still, these dependences can be easily mapped and therefore do not add to the uncertainty.

One main outcome of this careful investigation, apart from the best fit values of the contact parameters (and the methodology used to obtain them), is an increased awareness of the limits and capabilities of heuristic contact models. The logical next step, the author is now working on, is the assessment of the influence that the uncertainty on contact parameters has at the blade response level.

Nomenclature

Variables, matrices and vectors

β	Rotation
CF	Centrifugal force
{F}	Generic force vector
k	Stiffness
M	Moment produced by left contact force
[M], [K]	Mass and stiffness matrices
μ	Friction coefficient
nc	Number of contact points used to represent the flat-on-flat contact
t, n	Tangential and normal displacements at the contact
T, N	Tangential and normal contact forces
[T]	Transformation matrix
θ	Platform angle
u, w	Horizontal and vertical displacements
{U}	Vector of displacements
R	Damper radius

Additional subscripts

C	Contact
D	Damper
E	External
L, R	Left and right
P	Platforms
t, n	Aligned along the normal and tangential direction, respectively

Author details

Chiara Gastaldi

Address all correspondence to: chiara.gastaldi@polito.it

AERMEC Laboratory, Politecnico di Torino, Torino, Italy

References

[1] AAVV. High cycle fatigue under high profile study [Internet]. Available from: http://www.cordis.europa.eu/result/rcn/80294_en.html [Accessed: 2017-09-23]

[2] Griffin JH. Friction damping of resonant stresses in gas turbine engine Airfoils. Journal of Engineering for Power. 1980;**102**(2):329-333. DOI: 10.1115/1.3230256

[3] Srinivasan AV. Flutter and resonant vibration characteristics of engine blades. Journal of Engineering for Gas Turbines and Power. 1997;**119**(4):742-775. DOI: 10.1115/1.2817053

[4] Krack M, Salles L, Thouverez F. Vibration prediction of bladed disks coupled by friction joints. Archives of Computational Methods in Engineering. 2017;**24**(3):589-636

[5] Schwingshackl CW, Petrov EP, Ewins DJ. Effects of contact interface parameters on vibration of turbine bladed disks with underplatform dampers. Journal of Engineering for Gas Turbines and Power. 2012;**134**(3):032507. DOI: 10.1115/1.4004721

[6] Nacivet S, Pierre C, Thouverez F, Jezequela L. A dynamic Lagrangian frequency–time method for the vibration of dry-friction-damped systems. Journal of Sound and Vibration. 2003;**265**(1):201-219. DOI: 10.1016/S0022-460X(02)01447-5

[7] Herzog A, Krack M, Panning-von Scheidt L, Wallaschek J. Comparison of two widely-used frequency-time domain contact models for the vibration simulation of shrouded turbine blades. In: ASME Turbo Expo; June 16-20, 2014; Düsseldorf, Germany. 2014. p. V07BT33A018. DOI: 10.1115/GT2014-26226

[8] Pesaresi L, Salles L, Jones A, Green JS, Schwingshackl CW. Modelling the nonlinear behaviour of an underplatform damper test rig for turbine applications. Mechanical Systems and Signal Processing. 2017;**85**:662-679. DOI: 10.1016/j.ymssp.2016.09.007

[9] De Moerlooze K, Al-Bender F, Van Brussel H. A generalised asperity-based friction model. Tribology Letters. 2010;**40**(1):113-130

[10] Yang BD, Menq CH. Characterization of 3D contact kinematics and prediction of resonant response of structures having 3D frictional constraint. Journal of Sound and Vibration. 1998;**217**(5):909-925. DOI: 10.1006/jsvi.1998.1802

[11] Yang BD, Chu ML, Menq CH. Stick–slip–separation analysis and non-linear stiffness and damping characterization of friction contacts having variable normal load. Journal of Sound and Vibration. 1998;**210**(4):461-481. DOI: 10.1006/jsvi.1997.1305

[12] Petrov EP, Ewins DJ. Analytical formulation of friction interface elements. Journal of Turbomachinery. 2003;**125**(2):364-371. DOI: 10.1115/1.1539868

[13] Panning L, Sextro W, Popp K. Spatial dynamics of tuned and mistuned bladed disks with cylindrical and wedge-shaped friction dampers. International Journal of Rotating Machinery. 2003;**9**(3):219-228

[14] Petrov EP. Explicit finite element models of friction dampers in forced response analysis of bladed disks. Journal of Engineering for Gas Turbines and Power. 2008;**130**(2):022502

[15] Afzal M. On efficient and adaptive modelling of friction damping in bladed disks [dissertation]. KTH: 2017

[16] Cattaneo C. Sul contatto di due corpi elastici: distribuzione locale degli sforzi. Accademia dei Lincei. 1938

[17] Mindlin RD, Deresiewicz H. Elastic spheres in contact under varying oblique forces. Journal of Applied Mechanics. 1953;**20**:327-344

[18] Gastaldi C, Gola MM. On the relevance of a microslip contact model for under-platform dampers. International Journal of Mechanical Sciences. 2016;**115**:145-156. DOI: 10.1016/j.ijmecsci.2016.06.015

[19] Iwan WD. A distributed-element model for hysteresis. Journal of Applied Mechanics. 1966;**33**(4):893-900. DOI: 10.1115/1.3625199

[20] Menq CH, Bielak J, Griffin JH. The influence of microslip on vibratory response, part I: A new microslip model. Journal of Sound and Vibration. 1986;**107**(2):279-293. DOI: 10.1016/0022-460X(86)90238-5

[21] Csaba G. Modelling of a microslip friction damper subjected to translation and rotation. In: ASME, Turbo Expo 1999; June 7-10, 1999; Indianapolis, Indiana, USA. 1999. p. V004T03A012. DOI: 10.1115/99-GT-149

[22] Gaul L, Nitsche R. The role of friction in mechanical joints. Applied Mechanics Reviews. 2001;**54**(2):93-106. DOI: 10.1115/1.3097294

[23] Segalman D. A four-parameter Iwan model for lap-type joints. Journal of Applied Mechanics. 2005;**72**(5):752-760. DOI: 10.1115/1.1989354

[24] Rajaei M, Ahmadian H. Development of generalized Iwan model to simulate frictional contacts with variable normal loads. Applied Mathematical Modelling. 2014;**38**(15-16):4006-4018. DOI: 10.1016/j.apm.2014.01.008

[25] Botto D, Lavella M, Gola MM. Measurement of contact parameters of flat on flat contact surfaces at high temperature. In: ASME, editor. Turbo Expo. 2012

[26] Šanliturk KY, Stanbridge AB, Ewins DJ. Friction dampers: Measurement, modelling and application to blade vibration control. In: ASME, editor. Proc. Des. Eng. Conf.; 1995

[27] Schwingshackl CW, Petrov EP, Ewins DJ. Validation of test rig measure measurements and prediction tools for friction interface modelling. In: Turbo Expo; 2010

[28] Brändlein J, Eschmann P, Hasbargen L, Ball K. editors. Ball and Roller Bearings: Theory, Design, and Application. John Wiley and Sons; 1999

[29] Szwedowicz J, Gibert C, Sommer TP, Kellerer R. Numerical and experimental damping assessment of a thin-walled friction damper in the rotating setup with high pressure turbine blades. Journal of Engineering for Gas Turbines and Power. 2008;**130**(1):10

[30] Szwedowicz J. Bladed Disks: Non linear Dynamics. Structural Design of Aircraft Engines: Key Objectives and Techniques. Belgium: Seinturier & Paniagua Edition; 2008

[31] Sextro W. Dynamical Contact Problems with Friction. 1st ed. Berlin: Springer; 2007

[32] Siewert C, Panning L, Schmidt-Fellner A, Kayser A. The Estimation of the Contact Stiffness for Directly and Indirectly Coupled Turbine Blading. In: ASME, editor. Turbo Expo; 2006

[33] Allara M. A model for the characterization of friction contacts in turbine blades. Journal of Sound and Vibration. 2009;**320**(3):527-544

[34] Gastaldi C, Grossi E, Berruti TM. On the choice of contact parameters for the forced response calculation of a bladed disk with underplatform dampers. Journal of the GPPS. 2017;**1**:1-8

[35] Gastaldi C, Berruti TM. Method to solve the efficiency-accuracy trade-off of multi-harmonic balance calculation of structures with friction contacts. International Journal of Non-Linear Mechanics. 2017;**92**:25-40

[36] Szwedowicz J, Slowik S, Mahler A, Hulme CJ. Nonlinear dynamic analyses of a gas turbine blade for attainment of reliable shroud coupling. In: ASME, editor. Turbo Expo; 2005

[37] Gastaldi C, Gola MM. A random sampling strategy for tuning contact parameters of underplatform dampers. In: ASME, editor. Turbo Expo; 2015

[38] Pesaresi L, Stender M, Ruffini V, Schwingshackl CW. DIC measurement of the kinematics of a friction damper. In: SEM, editor. Dynamics of Coupled Structures. Conference Proceedings of the SEM. Vol. 4. Springer; 2017

[39] Gola MM, Liu T. A direct experimental–numerical method for investigations of a laboratory under-platform damper behavior. International Journal of Solids and Structures. 2014;**51**(25-26):4245-4259

[40] Gastaldi C, Gola MM. Preoptimization of underplatform dampers. Journal of Engineering for Gas Turbines and Power. 2016;**139**(GTP-16-1229):9